Geochemistry Geophysics Geosystems G3
AN ELECTRONIC JOURNAL OF THE EARTH SCIENCES
Published by AGU and the Geochemical Society

Article
Volume 7, Number 3
16 March 2006
Q03007, doi:10.1029/2005GC000962
ISSN: 1525-2027

Evolution of weathering patterns in the Indo-Burman Ranges over the last 280 kyr: Effects of sediment provenance on $^{87}Sr/^{86}Sr$ ratios tracer

C. Colin
Laboratoire des Interactions et Dynamique des Environnements de Surface (IDES), UMR 8148, CNRS-Université de Paris-Sud, Bâtiment 504, F-91405 Orsay Cedex, France (colin@geol.u-psud.fr)

L. Turpin, D. Blamart, N. Frank, and C. Kissel
Laboratoire des Sciences du Climat et de l'Environnement (LSCE), Laboratoire Mixte CEA/CNRS/UVSQ, Avenue de la Terrasse, F-91198 Gif-sur-Yvette Cedex, France

S. Duchamp
Laboratoire des Interactions et Dynamique des Environnements de Surface (IDES), UMR 8148, CNRS-Université de Paris-Sud, Bâtiment 504, F-91405 Orsay Cedex, France

[1] A high-resolution study of mineralogy and major element geochemistry combined with Sr and Nd isotopes has been conducted on high sedimentation rate cores collected off the Irrawaddy River mouth in the Andaman Sea and the Bay of Bengal to reconstruct the erosional and weathering history of the Irrawaddy River basin. In both cores, εNd(0) values imply that both glacial and interglacial sediments share a common crustal source: the Irrawaddy River. Strong glacial/interglacial cycles are recorded by $^{87}Sr/^{86}Sr$: interglacial periods yield values between 0.713 and 0.717, whereas glacial periods show higher values between 0.717 and 0.719. Variations of the pedogenic clays (smectite and kaolinite) to primary mineral (feldspar, quartz, illite, and chlorite) ratios show strong precessional cycles, suggesting a control by past changes in the summer monsoon intensity. Each increase in pedogenic clays content is also associated with a net loss of labile elements (Na, K, and Ca) from the detrital minerals under chemical weathering. Wet periods of summer monsoon reinforcement correspond to an increase in weathering of the Irrawaddy plain soils and a decrease of $^{87}Sr/^{86}Sr$ ratio. Plotting $^{87}Sr/^{86}Sr$ versus $^{87}Rb/^{86}Sr$ gives a pseudo-isochrons interpreted as a mixing line representing the strength of chemical weathering. During glacial stages, enhanced physical erosion induced by glacier scour and frost action in the highland of the Irrawaddy River basins produced high volumes of unaltered, Rb-rich minerals. The low sea level of glacial times constricted the river to the main channel in the lower reaches and permitted an efficient transport of unaltered Rb-rich minerals with high radiogenic Sr composition from the high relief of the Indo-Burman Ranges and the Tibetan plateau to the Indian Ocean.

Components: 9219 words, 11 figures, 1 table.

Keywords: Sr and Nd isotopes; major elements; erosional history; Indo-Burman Ranges; Irrawaddy River.

Index Terms: 1039 Geochemistry: Alteration and weathering processes (3617); 1040 Geochemistry: Radiogenic isotope geochemistry; 1050 Geochemistry: Marine geochemistry (4835, 4845, 4850); 1620 Global Change: Climate dynamics (0429, 3309); 0330 Atmospheric Composition and Structure: Geochemical cycles (1030)

Received 8 March 2005; **Revised** 1 September 2005; **Accepted** 28 November 2005; **Published** 16 March 2006.

Colin, C., L. Turpin, D. Blamart, N. Frank, C. Kissel, and S. Duchamp (2006), Evolution of weathering patterns in the Indo-Burman Ranges over the last 280 kyr: Effects of sediment provenance on $^{87}Sr/^{86}Sr$ ratios tracer, *Geochem. Geophys. Geosyst.*, *7*, Q03007, doi:10.1029/2005GC000962.

1. Introduction

[2] The high elevation of the Tibetan plateau and the Himalayas profoundly affects both the temperature structure of the atmosphere responsible for the seasonal winds and the location of the Indian monsoon rainfall. The Indian monsoon results from differential land-sea heating [*Webster*, 1987] and is characterized by a seasonal switch in wind direction, precipitation and run-off. It is also a major determinant of land vegetation over Southern Asia. During the last 1 my, low latitude solar insolation, driven by precession and eccentricity of the Earth's orbit, is considered to have been the main factor controlling Indian monsoon intensity [*Clemens and Prell*, 1990; *Clemens et al.*, 1991; *Colin et al.*, 1998; *Duplessy*, 1982].

[3] Much of the sediment derived from erosion of the Himalayas is well preserved, especially in the Bay of Bengal and the Arabian Sea, providing an opportunity to examine how clastic sediments record paleoenvironmental variations affecting the Himalayan and Indo-Burman Ranges [*Clift et al.*, 2002; *Colin et al.*, 1999; *Derry and France-Lanord*, 1996, 1997; *France-Lanord et al.*, 1993] and allow for the reconstruction of Indian monsoon history [*Colin et al.*, 1998]. On a geological timescale, changes in the strength of the Indian monsoon represent an important process driving chemical and/or physical weathering of the Himalayas and Indo-Burman Ranges and thus sediment supply to the ocean. Such variations, combined with changes of land configuration and sea level, are likely to influence detrital input to the Bay of Bengal and the Andaman Sea and will thus modify the provenance, grain size, and mineralogical composition of the sediment at any given site. Concurrently, it is reasonable to predict cyclic changes in weathering intensity and erosion of the Indo-Burman Ranges linked to monsoon strength.

[4] This paper reports on a high-resolution study of sedimentology, mineralogy and Sr-Nd isotopic data of two deep-sea gravity cores from the Andaman Sea and the Bay of Bengal (MD77-169 and MD77-176), in order to determine the effect of climatic changes (sea level and/or monsoon rainfall variations) on weathering and erosion of the Indo-Burman Ranges over the last two glacial/interglacial cycles (last 280 kyr).

[5] To obtain information on sediment sources and constrain transport processes of detrital sediments in the Andaman Sea and the Bay of Bengal, Sr and Nd isotope compositions were analyzed. Nd isotopic ratios are proven tracers for provenance studies of continental detritus [*Goldstein and Jacobsen*, 1988; *Tütken et al.*, 2002; *Grousset et al.*, 1988]. In contrast, Sr isotopic compositions seem to be fractionated between mineralogically different grain-size fractions during the erosion and transport [*Dasch*, 1969; *Goldstein et al.*, 1984; *Tütken et al.*, 2002]. We combine Rb-Sr and Nd isotope investigations with siliciclastic grain-size, mineralogical and major element proxies to establish the effect of sediment transport by ocean current and/or weathering on the $^{87}Sr/^{86}Sr$ ratio in the detrital sediments.

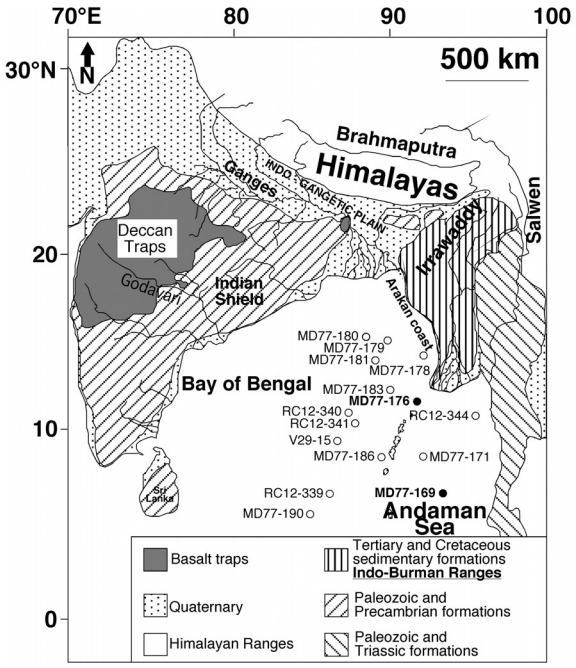

Figure 1. Schematic geological map of the Indian subcontinent and location of cores MD77-169 and MD77-176 investigated in detail in this study. The other cores are geographically distributed to ensure a good coverage of the Bay of Bengal and the Andaman Sea.

2. Materials and Methods

2.1. Core Locations

[6] Cores MD77-169 (10°12′5N–95°03′0E, 2360 m water depth) and MD77-176 (14°30′5N–93°07′6E, 1375 m water depth) were collected in the Andaman Sea during cruise OSIRIS III of the R.V. Marion Dufresne in 1977 (Figure 1). Core MD77-169 was taken on a seamount, in the central Andaman Sea, in order to avoid slope deposits such as turbidite or slumping. The lithology is homogeneous, dominated by olive grey terrigene-

ous muddy clay and nannofossil carbonate ooze. A grey volcanic ash layer is observed at 675 cm depth. Core MD77-176 is located near the continental slope 200 km away from the mouth of the Irrawaddy River (Figure 1). The lithology consists of intercalated olive grey terrigenous clay and silty clay layers with foraminifer- or nannofossil-bearing ooze.

2.2. Analytical Methods

[7] Quartz, kaolinite, feldspar and carbonate content of the bulk fraction were determined by Fourier Transform Infra-Red (FTIR) spectroscopy [*Pichard and Fröhlich*, 1986]. The samples were ground under acetone to a particle size of less than 2 μm with small agate balls in an agate vial, and kept at 4°C to prevent heating and structural changes. The powder was mixed with KBr in an agate mortar with a dilution factor of 0.25 wt%. A 300 mg pellet, 13 mm in diameter, was pressed into a vacuum die with up to 8 ton cm^{-2} of compression. 50 scans of Infrared spectra per sample cumulated in the 4000–250 cm^{-1} energy range with a 2 cm^{-1} resolution, were recorded using a Perkin-Elmer FT 16 PC spectrometer. Kaolinite and quartz proportions have been corrected for carbonate dilution using the following relationship: $[Min_{cor.}\% = Min_{mes.}\%/(100 - CaCO_3\%) \times 100]$.

[8] Grain-size distribution measurements of carbonate-free sediments were carried out on a Coulter LS 130. Bulk sediments were first put in suspension in deionized water and gently shaken to achieve desegregation. Ultrasound was used before each analysis in order to prevent bubbles of gas in water that could affect the analyses. The suspension was then gently poured into the fluid module of the granulometer in order to analyze the carbonate-free fraction grain-size distribution. Sonication was not used to complete the sediment dispersion, as previous measurements have shown that the use of ultrasonic dispersion can break brittle minerals (e.g., micas).

[9] The $^{87}Sr/^{86}Sr$ and $^{143}Nd/^{144}Nd$ ratios and concentrations of Sr, Rb and Nd were performed using static multicollection on a Finnigan MAT-262 at the Laboratoire des Sciences du Climat et de l'Environnement (LSCE, CEA-CNRS, Gif/Yvette). Following the procedure described by *Colin et al.* [1999], samples were decarbonated by leaching with 20% acetic acid solution in an ultrasonic bath, then rinsed five times and centrifuged to eliminate the carbonate solution. Samples were dissolved in $HF\text{-}HClO_4$ and HNO_3-HCl mixtures. The first chemical separation utilized Biorad columns packed with AG50WX-8, 200–400 mesh cation exchange resin. Sr and Rb were then eluted with 2 N HCl and the light rare earth elements with 2.5 N HNO_3. The Sr fraction was purified on a 20 μl SrSpec® column consisting of a polyethylene syringe with a 4 mm Ø Millex® filter. Nd was isolated by reverse-phase chromatography on HDEHP-coated Teflon powder. $^{87}Sr/^{86}Sr$ ratios were corrected for mass fractionation using normalization to a $^{86}Sr/^{88}Sr$ ratio = 0.1194. Replicate analyses of NIST SRM987 (n = 18) during the study gave a mean $^{87}Sr/^{86}Sr$ of 0.710240 ± 0.000013 (2σ), close to its certified value of 0.710245. Similarly, $^{143}Nd/^{144}Nd$ ratio was corrected for mass fractionation using a normalization to the natural $^{146}Nd/^{144}Nd$ ratio = 0.7219. Replicate analyses (n = 15) of a Johnson Matthey internal laboratory standard gave a mean $^{143}Nd/^{144}Nd$ of 0.511097 ± 0.000008, which corresponds to a value of 0.511849 for the La Jolla standard, and is comparable to its certified value of 0.511860. Uncertainties on concentration measurements for Sr, Rb and Nd are <0.1%. For convenience, Nd isotopic ratios results are expressed as $\varepsilon Nd(0) = [(^{143}Nd/^{144}Nd_{meas})/0.512638) - 1] \times 10000$, using the CHUR value given by *Jacobsen and Wasserburg* [1980].

[10] Major elements content analyses were performed on the carbonate-free fraction using an electron microprobe on glass samples obtained after fusion of the sediment following the methods described by *Colin et al.* [1998].

3. Chronological Framework

[11] The chronology of cores MD77-169 and MD77-176 has been established using Accelerator Mass Spectrometry (AMS) ^{14}C dates (based on monospecific samples of the planktonic foraminifera *Globigerinoides ruber*) and the $\delta^{18}O$ from planktonic foraminifera *G. ruber*, using the SPECMAP reference timescale [*Colin et al.*, 1998; *Duplessy*, 1982] (Figure 2). Core MD77-169 provides a continuous sedimentary record extending down to marine isotope stage (MIS) 8 (about 280,000 yr or 280 kyr) with an average linear sedimentation rate around 10.9 cm kyr^{-1} for the last 74 kyr and 3.9 cm kyr^{-1} for the older section. According to our oxygen isotope stratigraphy, the volcanic ash layer observed at 675 cm interval depth corresponds to the Youngest Toba Tuff (YTT, 74 kyr [*Chesner et al.*, 1991]). In core MD77-176, the sedimentary sequence represents

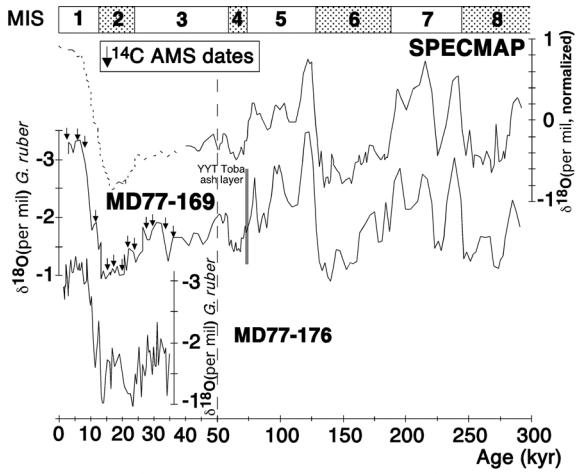

Figure 2. Planktonic foraminifera *G. ruber* (white) $\delta^{18}O$ record of cores MD77-169 and MD77-176. The timescales of both cores have been obtained by combining ^{14}C AMS ages and correlating with the SPECMAP isotopic record of *Martinson et al.* [1987].

the last 36 kyr (Figure 2). This core is characterized by higher accumulation rates (around 30 cm kyr^{-1}) than core MD77-169, consistent with its location in proximity to the continent.

4. Results

4.1. Siliciclastic Grain Size and Mineralogical Results

[12] Mean sizes of siliciclastic grains from core MD77-169 show variations between 5 and 32 μm, which are mostly in silt size (Figure 3b). However, a detailed examination of this curve indicates that interglacial stages are characterized, on average, by slightly larger grains (~10–32 μm for marine isotopic stages (MIS) 1 and 5) than glacial periods (~5–15 μm for MIS 2, 3, 4 and 6). Moreover, the beginning of the Holocene as well as the interglacial isotopic substages 5.1, 5.3 and 5.5 are characterized by a slightly coarser grain size (Figure 3b).

[13] Quartz, kaolinite and feldspar proportions vary significantly with MIS (Figure 3c). Long term fluctuations of quartz and feldspar contents are similar and range between 7–43% and 4–17%, respectively. On average lower values are observed during interglacial MIS 1, 5 and 7 than during glacial MIS 2, 3, 4, 6 and 8. Kaolinite content ranges between 3 and 26%. The kaolinite distribution is inversely correlated to those of quartz and feldspar with lower values during MIS 1 and 5 and the beginning of MIS 4, and higher values during warm isotopic substages 5.1, 5.3, 5.5, 7.1, 7.3 and 7.5 (Figure 3c).

[14] Because the FTIR analyses do not allow us to quantify all the major detrital minerals present in the sediment of core MD77-169, it is difficult to assign changes in the down-core record for any component due to the dilution of individual minerals by others (such as mica). Comparing two minerals using their ratio offers the advantage of reducing dilution effects. Kaolinite/feldspar, kaolinite/quartz and quartz/feldspar ratios as well as the smectite (illite/chlorite) obtained by *Colin et al.* [1999] on the clay size fraction (<2 μm) by XRD have been reported versus time in Figure 4. Down-core kaolinite/feldspar, kaolinite/quartz and quartz/feldspar ratios exhibit similar variations with higher values during the last 60 kyr, the beginning of MIS 5 and before 240 kyr. No systematic shift of these mineralogical ratios can be observed between glacial/interglacial shifts. However, these ratios present periodic variations as illustrated by the

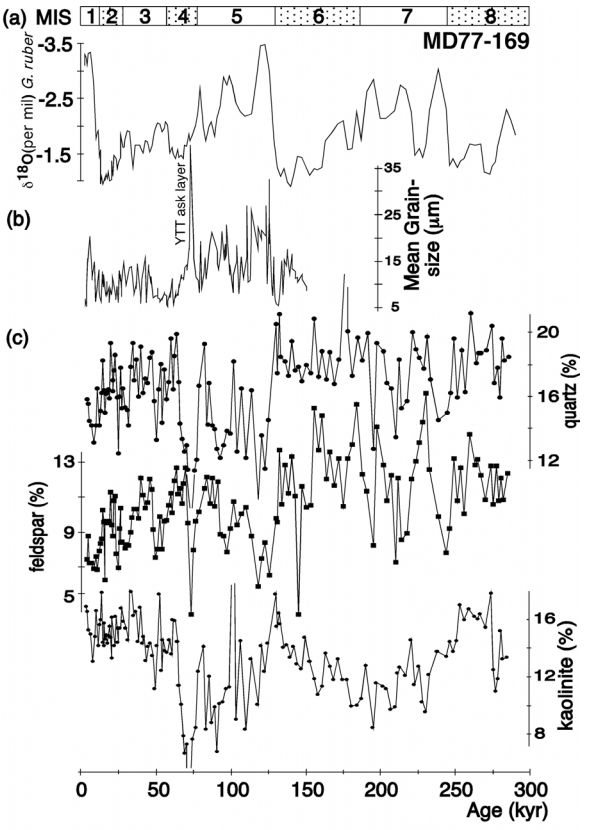

Figure 3. (a) Planktonic foraminifera *G. ruber* (white) $\delta^{18}O$ record of core MD77-169; (b) variation of mean grain-size (μm) of the siliciclastic fraction versus age (kyr); and (c) quartz, feldspar, and kaolinite proportion (%) on the bulk detrital fraction (corrected from carbonate dilution) versus age (kyr) for core MD77-169.

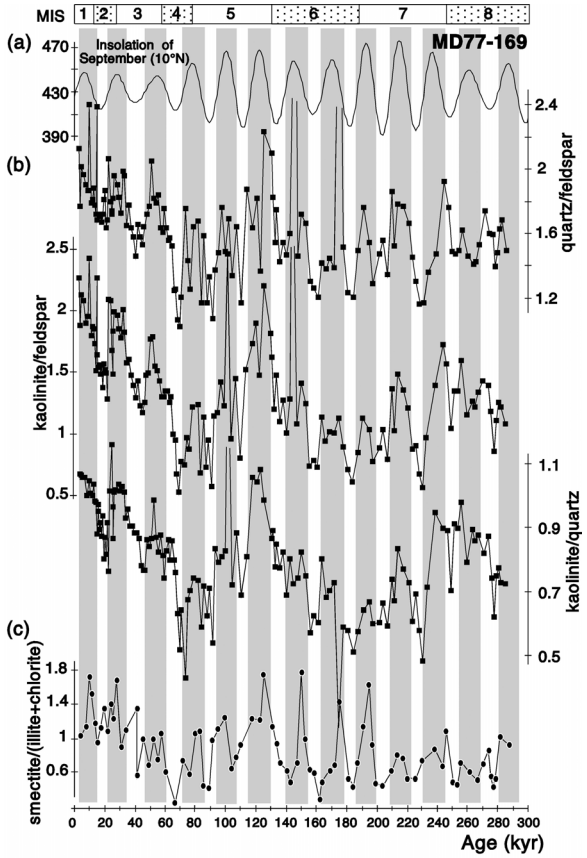

Figure 4. (a) Insolation curve calculated for September at latitude 10°N using Analyseries software [*Paillard et al.*, 1996]. (b) Quartz/feldspar, kaolinite/feldspar, and kaolinite/quartz versus age (kyr) for core MD77-169. (c) Smectite/(illite + chlorite) versus age (kyr) for core MD77-169 have been also reported for comparison [*Colin et al.*, 1999]. Shaded bands denote intervals of maximum insolation.

correlation between each of these mineralogical ratios and the solar radiation calculated at 10°N latitude for September (Figure 4a). September was chosen because it corresponds to the month giving an insolation curve in phase with the Indian monsoon variations as reconstructed by different proxies in the Arabian Sea [*Clemens and Prell*, 1991; *Beaufort*, 1996]. Each maximum of the insolation curve corresponds to an increase in these mineralogical ratios.

[15] Spectral analyses have been performed on these mineral variations using the Blackman-Tuckey methods with a Bartlett-type window providing a 80% confidence interval using the Analyseries software [*Paillard et al.*, 1996]. The power density spectra reported in Figure 5 show significant frequencies at 1/18 and 1/23 kyr^{-1} attributed to the precessional changes of the Earth's orbit. A frequency of 1/41 kyr^{-1} of the obliquity change is not observed in this core and the frequency at about 1/140 kyr^{-1} cannot be related to the orbital eccentricity (1/100 kyr^{-1}).

4.2. Major Element Results

[16] SiO_2/K_2O and K_2O/Al_2O_3 as well as the Chemical Index of Alteration (CIA = molar ratio of $[Al_2O_3/(Al_2O_3 + Na_2O + K_2O + CaO_{inorganic}) \times 100]$) [*Nesbitt and Young*, 1982] was calculated from the major element compositions (Figure 6). For primary minerals (non altered minerals), all feldspars have CIA value of 50 and the mafic minerals biotite, hornblende, and pyroxenes have CIA values between of 50-55, 10–30, and 0–10, respectively. Feldspar and mica weathering to smectite and kaolinite results in a net loss of K and Na in weathering profiles, whereas Al is resistant and is enriched in weathering products [*Nesbitt and Young*, 1982]. This induces an increase of CIA values of about 100 for kaolinite and 70–85 for smectite. The CIA value is thought to quantify the state of chemical weathering of the rocks by referencing the loss of labile elements such as Na, Ca, and K.

[17] K_2O/Al_2O_3 ratio varies also with the extent of weathering. K_2O/Al_2O_3 decreases when the chemical weathering of sediments increases. K_2O/SiO_2 may reflect the chemical weathering of the aluminosilicate fraction, but this ratio is also dependent on the initial proportion of quartz, a primary mineral strongly resistant to dissolution in most soils. Consequently, K_2O/SiO_2cor ratio of the aluminosilicate fraction has been calculated using quartz contents analyzed by FTIR (Figure 6).

[18] K_2O/SiO_2cor and K_2O/Al_2O_3 ratios, as well as CIA, vary significantly with climatic changes (Figure 6). In general, MIS 2, 3, 4, 6 and 8 are characterized by higher ratios of K_2O/SiO_2cor and K_2O/Al_2O_3 than the ones of interglacial MIS 1 and 5. On a shorter timescale, all the warm isotopic substages (5.1, 5.3, 5.5, 7.1, 7.3 and 7.5) are also characterized by a slight decrease of both ratios. Long-term changes of the CIA values do not show similar glacial-interglacial cycles, but they seem well correlated with solar insolation curve. Each peak of CIA value corresponds to a maximum in solar insolation. These results nicely correspond to the mineralogical ones as each cycle of the K_2O/Al_2O_3, K_2O/SiO_2cor and CIA is accompanied by a cycle of the low to high kaolinite/feldspar, kaolin-

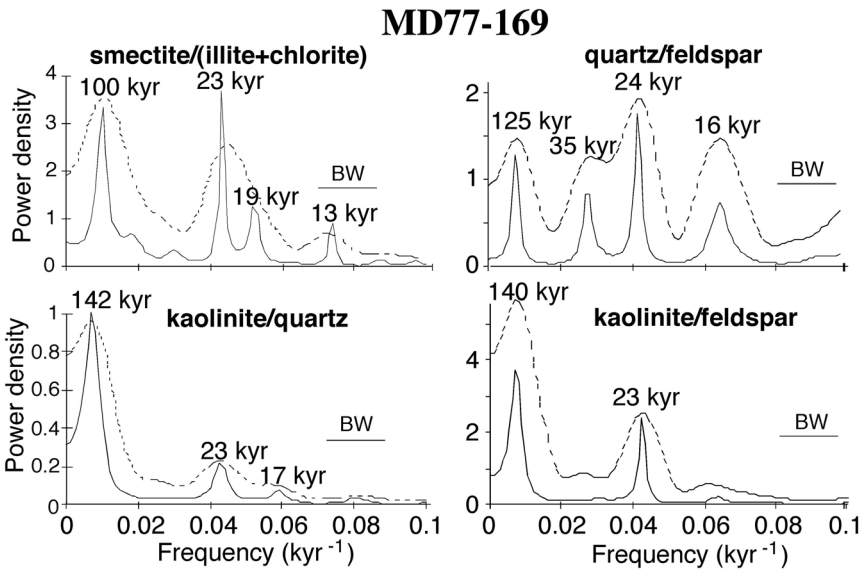

Figure 5. Periodograms of the smectite/(illite + chlorite), quartz/feldspar, kaolinite/quartz, and kaolinite/feldspar ratios for core MD77-169. Dashed line is Blackman-Tukey; solid line is maximum entropy. BW is the bandwidth.

ite/quartz, quartz/feldspar and smectite (illite/chlorite) ratios (Figure 6).

4.3. Isotopic Results

[19] $^{87}Sr/^{86}Sr$ ratios, εNd(0) values and concentrations of Rb, Sr and Nd measured on the cores MD77-169 and MD77-176 carbonate-free fraction are listed in Table 1. The ranges of Nd and Sr concentrations, 20.5–26.1 ppm Nd and 79.4–129.7 ppm Sr, are consistent with the previously published values for sediments from the Ganges-Brahmaputra and the Bay of Bengal [*Bouquillon et al.*, 1990; *Colin et al.*, 1999; *France-Lanord et al.*, 1993; *Galy and France-Lanord*, 2001; *Goldstein and Jacobsen*, 1988; *Pierson-Wickmann et al.*, 2001].

[20] In core MD77-169, the εNd(0) values range from −9.5 to −11, and $^{87}Sr/^{86}Sr$ ranges from 0.7140 to 0.7190 (Table 1 and Figure 7). With the exception of the beginning of the Holocene, no significant change in the εNd(0) values occur during the last 280 kyr. In contrast, glacial periods are characterized on average by higher radiogenic $^{87}Sr/^{86}Sr$ (0.717–0.719) than interglacials (0.714–0.717). In this core, the same relationship between glacial/interglacial periods and $^{87}Sr/^{86}Sr$ is also observed on a shorter timescale: three distinct minima of the $^{87}Sr/^{86}Sr$ are observed during MIS 5 and 7, coinciding with warm isotopic substages (5.1, 5.3, 5.5, 7.1, 7.3 and 7.5). Other minima of $^{87}Sr/^{86}Sr$ values are also observed during glacial stages around 30, 50 and 265 kyr.

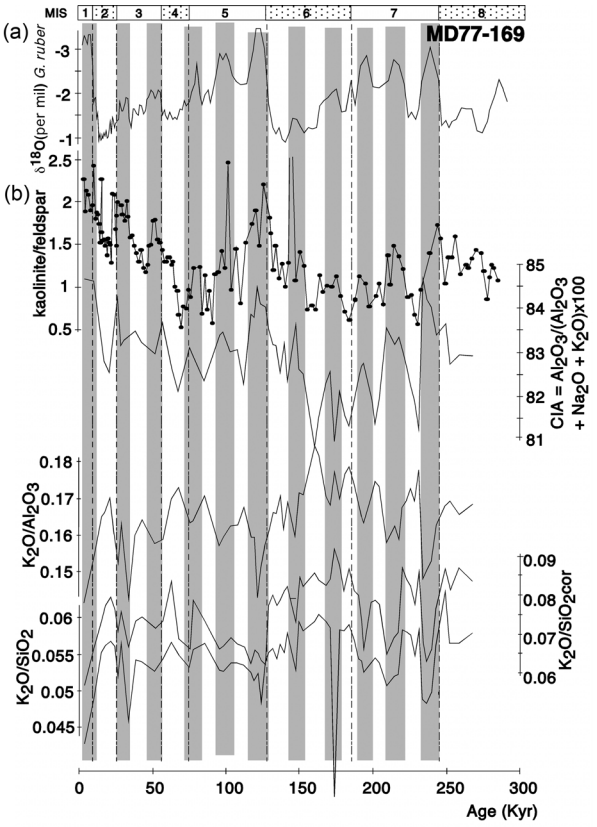

Figure 6. (a) Insolation curve calculated for September at latitude 10°N using Analyseries software [*Paillard et al.*, 1996]; (b) CIA, K_2O_3/SiO_2, K_2O_3/SiO_2cor, and K_2O_3/Al_2O_3 versus age (kyr) for core MD77-169. Kaolinite/feldspar ratio has also been reported for comparison. Shaded bands denote intervals of maximum insolation.

Table 1. Rb, Sr, and Nd Isotopic Data Measured on the Carbonate-Free Fraction of Core MD77-169 and MD77-176 Sediments[a]

Depth, cm	Age, kyr	Rb, ppm	Sr, ppm	$^{87}Rb/^{86}Sr$	$^{87}Sr/^{86}Sr$	Nd, ppm	$^{143}Nd/^{144}Nd$	εNd(0)
				MD77-169				
24	5.10	117.3	129.7	2.62	0.71434	24.0	0.512125	−10.0
83	8.87	131.0	117.9	3.21	0.71468	23.2	0.512153	−9.5
158	14.44	144.6	110.4	3.79	0.71669	23.5	0.512095	−10.6
250	22.18	154.5	96.6	4.63	0.71852	24.8	0.512096	−10.6
320	28.68	139.8	85.5	4.73	0.71857	24.0	0.512096	−10.6
360	32.66	132.5	101.3	3.79	0.71761			
410	37.95	161.7	95.9	4.88	0.71863	26.0	0.512101	−10.5
443	41.66	155.2	98.4	4.57	0.71785	24.1	0.512098	−10.5
500	48.54	144.8	104.0	4.03	0.71665	24.0	0.512080	−10.9
540	53.79	143.6	99.3	4.19	0.71744			
590	60.91	165.0	95.0	5.03	0.71926	25.8	0.512095	−10.6
630	67.10	166.0	99.7	4.82	0.71862	24.6	0.512093	−10.6
690	77.30	139.0	100.5	4.01	0.71801	24.8	0.512095	−10.6
710	80.97	141.1	112.5	3.63	0.71657	26.2	0.512099	−10.5
740	86.72	133.7	88.8	4.36	0.71736	20.5	0.512086	−10.8
780	94.90	157.2	116.7	3.90	0.71605	24.7	0.512096	−10.6
810	101.42	156.0	112.8	4.00	0.71617	24.3	0.512108	−10.3
830	105.96	149.1	111.8	3.86	0.71692	24.9	0.512108	−10.3
850	110.65	153.5	122.6	3.63	0.71639	24.6	0.512083	−10.8
870	115.50	150.7	124.0	3.52	0.71545	26.1	0.512082	−10.8
880	117.98	128.5	123.9	3.00	0.71540			
890	120.49	136.7	123.4	3.21	0.71542	24.8	0.512083	−10.8
920	128.27	146.6	98.5	4.31	0.71795	25.3	0.512079	−10.9
960	139.16	156.0	101.1	4.47	0.71847			
1000	150.61	144.1	94.4	4.42	0.71817	24.5	0.512099	−10.5
1045	164.12	153.2	101.7	4.36	0.71823	25.7	0.512121	−10.1
1070	171.89	159.0	96.8	4.76	0.71834	25.7	0.512098	−10.5
1080	175.04	126.7	79.4	4.62	0.71851			
1090	178.21	126.0	79.6	4.59	0.71876	22.9	0.512100	−10.5
1100	181.41	145.1	109.4	3.84	0.71812	25.6	0.512112	−10.3
1130	191.13	158.0	111.4	4.11	0.71772	25.8	0.512080	−10.9
1150	197.70	142.9	128.4	3.22	0.71537	25.2	0.512110	−10.3
1170	204.32	142.6	129.5	3.19	0.71584	25.2	0.512120	−10.1
1190	210.97	158.6	130.6	3.52	0.71489	24.6	0.512090	−10.7
1210	217.65	165.6	104.4	4.59	0.71714	25.7	0.512114	−10.2
1220	220.99	162.8	104.0	4.53	0.71715			
1230	224.33	141.1	113.0	3.62	0.71732	25.7	0.512099	−10.5
1250	231.00	168.1	114.7	4.25	0.71804			
1270	237.62	139.2	122.4	3.29	0.71477	25.3	0.512117	−10.2
1290	244.18	155.6	96.8	4.65	0.71771	25.0	0.512110	−10.3
1310	250.66	174.1	100.6	5.02	0.71825	26.1	0.512095	−10.6
1345	261.70	164.2	102.8	4.62	0.71777	26.0	0.512075	−11.0
1370	269.30	154.0	97.8	4.56	0.71876	26.7	0.512080	−10.9
1390	275.15	172.7	101.1	4.95	0.71842	25.6	0.512102	−10.5
1440	288.67	138.8	101.9	3.95	0.71767	25.7	0.512094	−10.6
				MD77-176				
17	1.89	124.7	113.0	3.19	0.71534	24.2	0.512162	−9.3
180	3.80	120.8	114.5	3.05	0.71477	23.8	0.512178	−9.0
295	6.20	113.2	101.3	3.23	0.71461	23.1	0.512207	−8.4
380	8.23	110.2	121.4	2.63	0.71358	24.5	0.512241	−7.7
475	10.91	108.9	98.2	3.21	0.71526	22.6	0.512197	−8.6
590	14.78	123.5	90.9	3.94	0.71777	22.7	0.512209	−8.4
638	16.43	139.1	95.2	4.23	0.71792	24.2	0.512179	−9.0
700	20.72	142.9	101.6	4.07	0.71705	23.8	0.512186	−8.8
780	26.11	118.2	98.5	3.48	0.71729	24.4	0.512180	−8.9
852	30.18	108.0	98.5	3.18	0.71720	24.7	0.512192	−8.7
952	33.93	151.5	109.0	4.02	0.71630	24.9	0.512168	−9.2

[a] Nd results are expressed as εNd(0) = $[((^{143}Nd/^{144}Nd_{meas})/0.512638) - 1] \times 1000$, using the present-day CHUR value of *Jacobsen and Wasserburg* [1980].

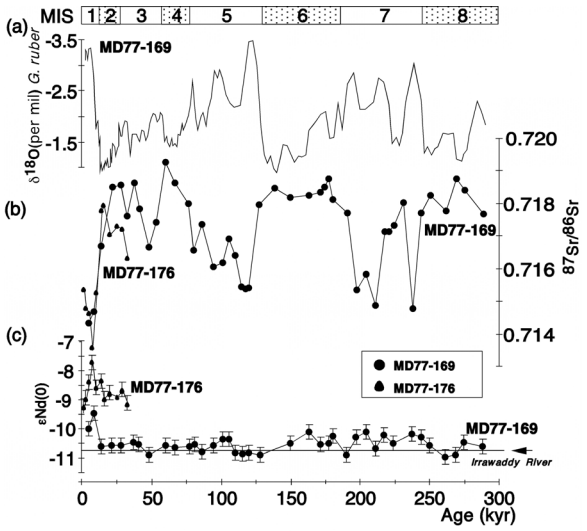

Figure 7. (a) Planktonic foraminifera *G.ruber* $\delta^{18}O$ record versus age (kyr). (b) $^{87}Sr/^{86}Sr$ ratios and (c) $\varepsilon Nd(0)$ values measured on the carbonate-free fraction versus age (kyr) for cores MD77-169 and MD77-176.

[21] In core MD77-176, on a short timescale, the $\varepsilon Nd(0)$ and $^{87}Sr/^{86}Sr$ values exhibit the same pattern (Table 1 and Figure 7) as in core MD77-169. The $\varepsilon Nd(0)$ values are higher (between -7.5 and -9.5) than those of core MD77-169 but do not present any significant variations during the last 34 kyr, except for the beginning of the Holocene. The last glacial period sediments (between 0.717 and 0.719) are also characterized by higher $^{87}Sr/^{86}Sr$ than the Holocene (between 0.713 and 0.716).

5. Discussion

5.1. Sediment Sources

[22] The paleoclimatic interpretation of mineralogical and detrital geochemical records requires knowledge of the potential source areas, as well as the mode and strength of the transport processes involved [*Gingele et al.*, 1998; *Wehausen and Brumsack*, 2002]. The Nd isotopic composition and to a lesser extent the $^{87}Sr/^{86}Sr$ can be used as reliable tracers of source for sediments deposited in the Bay of Bengal and the Andaman Sea [*Bouquillon et al.*, 1990; *France-Lanord et al.*, 1993].

[23] Variations in $\varepsilon Nd(0)$ versus $^{87}Sr/^{86}Sr$ for cores MD77-169 and MD77-176 sediments are presented in Figure 8. In such diagrams, mixing of sediments from two different sources generates a hyperbolic trend between end-members, the shape of which depends on end-member Sr/Nd ratio. As long as source rocks have similar Sr/Nd and the sedimentary products experienced similar weathering histories, their Sr/Nd ratios will be similar and the curvature of their mixing hyperbolae will be low. Three sediment sources have been identified [*Colin et al.*, 1999]: (1) Ganges/Brahmaputra Rivers, (2) Irrawaddy River, and (3) sediments derived from the western part of the Indo-Burman Ranges. This last end-member was established by *Colin et al.* [1999] using Sr and Nd isotopic compositions mapping of modern and LGM sediments from the Bay of Bengal and Andaman Sea. Sediments located close the Arakan coast (Figure 1) were used to determine the isotopic composition of sediments deriving from the Indo-Burman Ranges. These three end-members are shown in Figure 8.

[24] For both cores, the isotopic composition of glacial and interglacial sediments can be distinguished (Figure 8). The isotopic composition of the interglacial sediments from core MD77-169 ($0.7143 < ^{87}Sr/^{86}Sr < 0.7177$; $-9.5 < \varepsilon Nd(0) < -10.9$) falls in the field of the isotopic composition of the Andaman Sea sediments ($0.7123 < ^{87}Sr/^{86}Sr < 0.7172$; $-9.2 < \varepsilon Nd(0) < -11.5$) and one modern Irrawaddy River sample ($^{87}Sr/^{86}Sr$ = 0.7133 and

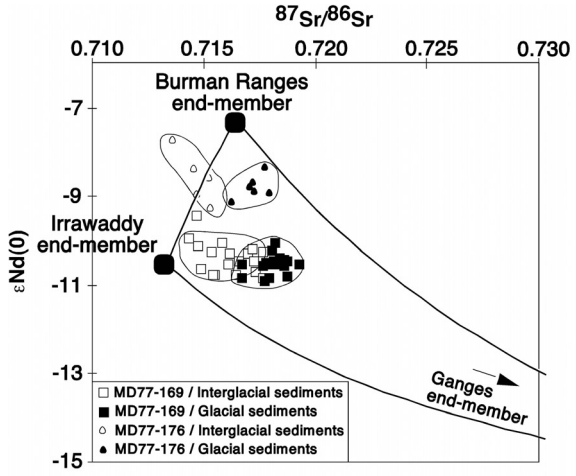

Figure 8. $^{87}Sr/^{86}Sr$ versus $\varepsilon Nd(0)$ diagram indicating the isotopic distribution of both interglacial and glacial samples from cores MD77-169 and MD77-176. The Irrawaddy River end-member corresponds to the isotopic composition of one modern Irrawaddy River sample [*Colin et al.*, 1999]. The Ganges end-member is obtained using the Sr and Nd isotopic composition of Ganges River sediments [*France-Lanord et al.*, 1993; *Galy and France-Lanord*, 2001]. The Indo-Burman Ranges end-member has been established by *Colin et al.* [1999], and it corresponds to Sr and Nd isotopic compositions of sediments from the Arakan coast (Figure 1) deriving from the physical erosion of the Indo-Burman Ranges.

εNd(0) = −10,7 [*Colin et al.*, 1999]). The isotopic signatures of glacial sediments are characterized by a slight increase of the $^{87}Sr/^{86}Sr$ ratios but do not show any change in the εNd(0) values. These glacial/interglacial shifts have also been observed for the Andaman sea sediments [*Colin et al.*, 1999].

[25] The εNd(0) values are unlikely to be significantly modified during chemical weathering on land [*Borg and Banner*, 1996] and are further considered insensitive to grain-size sorting during transport [*Tütken et al.*, 2002; *Goldstein and Jacobsen*, 1988]. In contrast, previous studies have shown that $^{87}Sr/^{86}Sr$ ratios are influenced by grain-size effects [*Dasch*, 1969; *Tütken et al.*, 2002]. This implies that the εNd(0) values are more reliable tracers of the provenance of sediments than the $^{87}Sr/^{86}Sr$ ratio [*Tütken et al.*, 2002]. Because the εNd(0) values do not show any significant change downcore, we suggest that the Irrawaddy River is the main contributor of detrital material to core MD77-169 during the last two glacial/interglacial cycles.

[26] Furthermore, if we consider that during glacial periods the isotopic compositions of the three end-members are similar to the present-day conditions, such a shift would imply a slightly higher contribution of sediments deriving from the Ganges during glacial periods. However, the water depths in most of the straits between the Andaman and Nicobar islands (Figure 1) are quite shallow and a decrease of 60 m would be enough to cut most of the water exchange between the Andaman Sea and the Bay of Bengal. During glacial times, the Andaman Sea was almost completely isolated due to low sea level, and sediments from the Ganges River could not have reached it.

[27] Core MD77-176 sediments are characterized by slightly higher εNd(0) values (between −7.5 and −9.5) implying that the sediment provenances are different to those of core MD77-169 (Figure 8). The Sr and Nd isotopic compositions for Holocene sediments of this core are similar to those of the eastern Bay of Bengal sediments and are located on a mixing hyperbola linking two end-members. One of them corresponds to the isotopic composition of a sediment sample recovered in the Irrawaddy River. The second end-member of the mixing curves indicates a contribution of sediment with low radiogenic Nd ratios derived from the Indo-Burman Ranges. As for core MD77-169, glacial sediments from core MD77-176 are characterized by higher $^{87}Sr/^{86}Sr$ ratios than interglacial sediments. However, considering only the εNd(0) values, the proportion of these two end-members, which present a distinctive set of isotopic characteristics (εNd(0) = −10.7 for the Irrawaddy River sediments, and around −8 for the Indo-Burman Ranges [*Colin et al.*, 1999]), does not vary significantly through time, suggesting no important changes of the sedimentary sources.

5.2. Erosional History of the Indo-Burman Ranges

[28] Variations in the mineralogical composition of the surface and Quaternary sediments of the Bay of Bengal and the Andaman Sea do not match variations in the lithological or diagenetic states. Thus the primary control on such variations is provenance [*Bouquillon et al.*, 1989, 1990; *Colin et al.*, 1999; *Fagel et al.*, 1994]. Because the core MD77-169 received mainly sediment from the Irrawaddy River at least during the last two climatic cycles (260 kyr), downcore mineralogical variations can be used to reconstruct the erosional history of the Indo-Burman Ranges.

[29] Sea level variations occurring during the transition between glacial and interglacial stages may have had an important control in the distribution of sediments from the Irrawaddy and Ganges-Brahmaputra Rivers to the open ocean. During low sea level stands, the continental shelf was exposed and fluvial sediments were funneled directly to the deep sea. In contrast, it has been demonstrated for wide continental shelves that, during high sea level, sediment is trapped in the delta and adjacent shelf, and coarse clastic deposition is cut off in the deep sea. Such results have been obtained for the large continental shelf off the Pearl River and Mekong River mouth [*Boulay et al.*, 2003; *Liu et al.*, 2005]. Grain size variations of the core MD77-169 are not in agreement with this scheme because they display coarser grain size during interglacial stages (Figure 3b and 7). Furthermore, glacial/interglacial changes are not associated with variations of the kaolinite/feldspar, kaolinite/quartz, quartz/feldspar and smectite/(illite + chlorite) ratios (Figure 6). This suggests that sea level changes do not directly control the detrital input to the Andaman Sea. Most of sediment from the Irrawaddy River could be transported rapidly seaward with no significant accumulation on the narrow continental shelf in front of the Irrawaddy mouth. In addition, numerous studies on the shelf and continental slope from the Northern Bay of Bengal show that some Ganges-Brahmaputra River sediments bypass the

narrow Bengal Shelf during high sea level periods [*Kuehl et al.*, 1989; *Weber et al.*, 2002].

[30] Numerous paleoclimatic studies have shown a relation between summer insolation changes on the Tibetan plateau and the intensity of the winter and summer Indian monsoon [*Clemens and Prell*, 1991; *Clemens et al.*, 1991]. Consequently, the strong precessional signal observed in mineralogical variations (Figure 5), the correlation between the mineralogical changes and the insolation curve (Figure 4) imply that the detrital input to the Andaman Sea is mainly control by changes of the summer and/or winter Indian monsoon intensity. Such a relationship has already been observed in sedimentary records from the western Indian Ocean [*Clemens et al.*, 1991] and the South China Sea [*Boulay et al.*, 2005].

[31] In the northern part of the Indian Ocean, an increase of the summer insolation is associated with an intensification of the summer (SW) monsoon and a reduction of the winter (NE) monsoon [*Duplessy*, 1982; *Clemens and Prell*, 1991; *Clemens et al.*, 1991]. Such changes could be characterized by (1) an intensification of the SW winds and the dominant sea surface current associated with summer monsoon in the Bay of Bengal [*Duplessy*, 1982; *Fontugne and Duplessy*, 1986] and (2) a reinforcement in the intensity of monsoon rainfall on the Himalayan and Indo-Burman river basins [*Duplessy*, 1982].

[32] A change in the dominant sea surface current in the Andaman Sea, associated with a modification of the intensity of the summer and winter monsoons, may have had an impact on the efficiency of the transport of coarse minerals to core MD77-169. Such processes are consistent with the observed grain size variations in the core MD77-169. Each period of intensification of the Indian summer monsoon is associated with an increase in the mean grain size in core MD77-169 in agreement with the expected increased runoff in the Irrawaddy River basin, as well as the intensification of sea surface circulation associated with the summer monsoon. In addition, such changes in the dominant sea surface circulation would also be associated with variations in the sediment sources. This hypothesis is not supported by either cores, nor is it by the Andaman Sea and eastern Bay of Bengal sediments [*Colin et al.*, 1999], which present no evidence in sediment provenance changes on glacial/interglacial timescales.

[33] Furthermore, systematic mineralogical variations occur at the same time in the coarse detrital fraction and in the clay (<2 μm) fraction (Figure 4). Consequently, the observed variations cannot be attributed to mineralogical fractionation caused by a more or less efficient transport of coarse material to the Andaman Sea following changes of sea-surface current intensity. Thus the downcore mineralogical changes of core MD77-169 reflect mainly those of the Irrawaddy River input and seem to be independent from sea-surface current pattern. To better understand the cause of systematic mineralogical variations, it is necessary to document the origins and source areas of the minerals present in the Irrawaddy River basin. In our context, two groups of minerals can be distinguished:

[34] First group: Feldspars, quartz, illite and chlorite. Feldspars and quartz are abundant in igneous and metamorphic formations. Illite derives from the degradation of micas in igneous and metamorphic rocks [*Chamley*, 1989]. Chlorite is also a common "primary" mineral in low-grade metamorphic rocks. Such rocks are common in Palaeozoic and Triassic crystalline formations located in the Indo-Burman Ranges [*Bender*, 1983]. These minerals are considered as mainly primary minerals and are derived from physical erosion or moderate chemical weathering of the highlands of the Irrawaddy River basin.

[35] Second group: Smectite and kaolinite. Kaolinite and smectite are readily found in soils of intertropical landmass characterized by a warm, humid climate, and their concentrations therefore display a strong climatic dependence controlled by the intensity of continental hydrolysis [*Chamley*, 1989]. Kaolinite is common on steep slopes within the basin under good drainage conditions, whereas smectite is formed in confined environments, by recombination of released cations. Smectite is not formed in the same part of the river basin as kaolinite. However, both smectite and kaolinite are abundant in the Irrawaddy plain soils [*Ségalen*, 1995] where Himalayan material is deposited and altered. These minerals are formed by hydrolysis of feldspars, illite and chlorite minerals [*Chamley*, 1989].

[36] Consequently, first to second group mineral ratios (kaolinite/quartz, kaolinite/feldspar and smectite/(illite + chlorite)) can be used as proxies of the intensity of chemical weathering in the Irrawaddy plain soils. Given the higher sensitivity of feldspar to chemical weathering than quartz, it can be reasonably assumed that quartz/feldspar ratio behaves in the same way as the other ratios.

[37] In addition, each increase of the kaolinite/quartz, kaolinite/feldspar and smectite/(illite + chlorite) ratios is accompanied respectively by a decrease of the K_2O/Al_2O_3 and K_2O/SiO_2cor and by an increase of the CIA (Figure 6). An increase of secondary minerals both in the silt or clay fractions correspond to an increase in the intensity of weathering of detrital minerals by loss of labile elements.

[38] For core MD77-169, an increase of summer monsoon rainfall is predicted to be characterized by an increase of kaolinite/quartz, kaolinite/feldspar, quartz/feldspar and smectite/(illite + chlorite) ratios. We interpret these mineralogical variations as an increase in the chemical weathering associated with wetter conditions in the Irrawaddy floodplain during periods of stronger summer monsoon rainfall. This would favor soil development and thus the production of smectite and kaolinite. This process would imply that soil production is sufficiently rapid (<3 kyr) to explain the rapid changes observed in the Andaman sediment due to climatic forcing. *Thiry* [2000] argued that sequential changes in sedimentary clay mineral assemblages with periods of less than 1 Myr cannot be caused by climatic changes acting on soil mineralogy. However, recent investigations on chemical weathering of South Indian watersheds, have revealed that weathering rates can reach ~150 kg/ha/yr [*Oliva et al.*, 2003] allowing short-term changes of the chemical weathering to be recorded in marine sediments [*Liu et al.*, 2004, 2005]. Furthermore, numerous studies attest that the main clay mineral transformations (such as smectite) occur within the early few kyr of soils development [*Egli et al.*, 2001].

5.3. Alteration of Strontium Isotopic Compositions During Weathering

[39] In both cores MD77-169 and MD77-176, glacial sediments are characterized by higher $^{87}Sr/^{86}Sr$ ratios than interglacial sediments (Figure 7). Previous studies have shown that Sr isotopic compositions are influenced by grain-size effect [*Dasch*, 1969; *Tütken et al.*, 2002]. In most cases, an increase of grain-size is associated with higher radiogenic Sr ratios.

[40] In core MD77-169, downcore variations of the $^{87}Sr/^{86}Sr$ ratios are not correlated with the mean grain size variations (Figure 3a), suggesting that the $^{87}Sr/^{86}Sr$ cannot only be attributed to grain-size effects. In addition, these glacial/interglacial shifts of $^{87}Sr/^{86}Sr$ ratios are also observed in last glacial maximum and Holocene sediments of the Andaman Sea and Eastern Bay of Bengal [*Colin et al.*, 1999]. Most of the last glacial maximum sediments are characterized by similar εNd(0) values and higher $^{87}Sr/^{86}Sr$ ratios than Holocene sediments [*Colin et al.*, 1999].

[41] In core MD77-169, each period of intensification of the chemical weathering, as reconstructed by mineralogical investigations, is associated with a decrease in the $^{87}Sr/^{86}Sr$ ratios. This correlation between the $^{87}Sr/^{86}Sr$ and mineralogical proxies or CIA values variations is not linear because the $^{87}Sr/^{86}Sr$ also shows strong glacial/interglacial cycles, which are not as well observed in the mineralogical ratios changes. However, in other cores located on the Andaman Sea and the Bay of Bengal (MD77-176, RC12-344, MD77-180 and MD77-183), glacial sediments are characterized by higher contents of primary minerals (illite and chlorite) and lower contents of pedogenic clays (smectite and kaolinite) [*Bouquillon et al.*, 1989; *Bouquillon*, 1987; *Colin et al.*, 1999; *Fang*, 1987].

[42] Moreover, in core MD77-169, $^{87}Sr/^{86}Sr$ ratios show moderate correlations with Sr/Al ($r = -0.80$) and K_2O/Al_2O_3 ($r = 0.54$) (Figure 9). Glacial MIS 2, 3, 4 and 6 are characterized by higher K_2O/Al_2O_3 and lower Sr/Al ratios than interglacial MIS 1, 5 and 7, implying higher contents of high-Rb, low-Sr minerals such as potassium feldspar and biotite in glacial sediments. Such detrital minerals have been identified by microscopic observations and XRD analyses of cores MD77-169 and MD77-176 sediments, but unfortunately, only potassium feldspar (orthoclase) can be analyzed by FTIR (Figure 3b).

[43] $^{87}Sr/^{86}Sr$ versus $^{87}Rb/^{86}Sr$ measured in cores MD77-169 and MD77-176 sediments are reported in Figure 10 with a compilation of previously published data from Bay of Bengal and Andaman Sea sediments. For both cores, all sediment samples form a regular linear array. This pseudo-isochron gives an apparent age of 155 ± 20 Ma ($^{87}Sr/^{86}Sr_i = 0.7082 \pm 0.0008$) without any geological meaning. Glacial sediments can be distinguished from interglacial because of their higher $^{87}Sr/^{86}Sr$ and $^{87}Rb/^{86}Sr$ ratios. This is in agreement with higher content of high-Rb and low-Sr minerals found in glacial sediments. With the exception of one core (MD77-180), similar linear trends and glacial/interglacial shifts are observed in all the cores from the Bay of Bengal and the Andaman Sea (Figure 10). This correlation cannot be interpreted as a mixing between two end-members

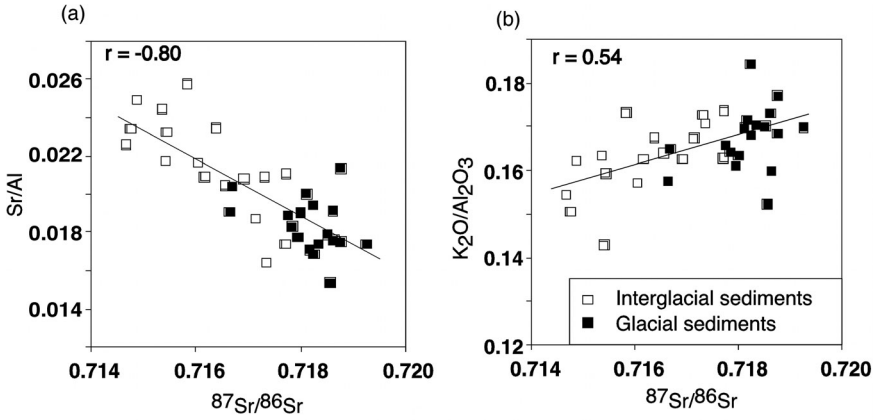

Figure 9. (a) K_2O/Al_2O_3 versus $^{87}Sr/^{86}Sr$ diagram and (b) Sr/Al_2O_3 versus $^{87}Sr/^{86}Sr$ diagram for core MD77-169.

because the εNd(0) values do not present any significant shift between the different potential end-members, which have been characterized by a distinctive set of isotopic characteristics.

[44] These results imply that the climatic trend of the $^{87}Sr/^{86}Sr$ is independent from (1) the provenance of sediments which is different in the Andaman Sea and in the eastern part of the Bay of Bengal; (2) the distance of the sediments from the feeding river mouths; and (3) the lithology and grain size of the sediments.

[45] Consequently, the downcore Sr isotopic composition of both cores can be attributed to glacial/interglacial shifts of sediment mineralogy induced by a change in the weathering patterns on the continent. The $^{87}Sr/^{86}Sr$ change during weathering

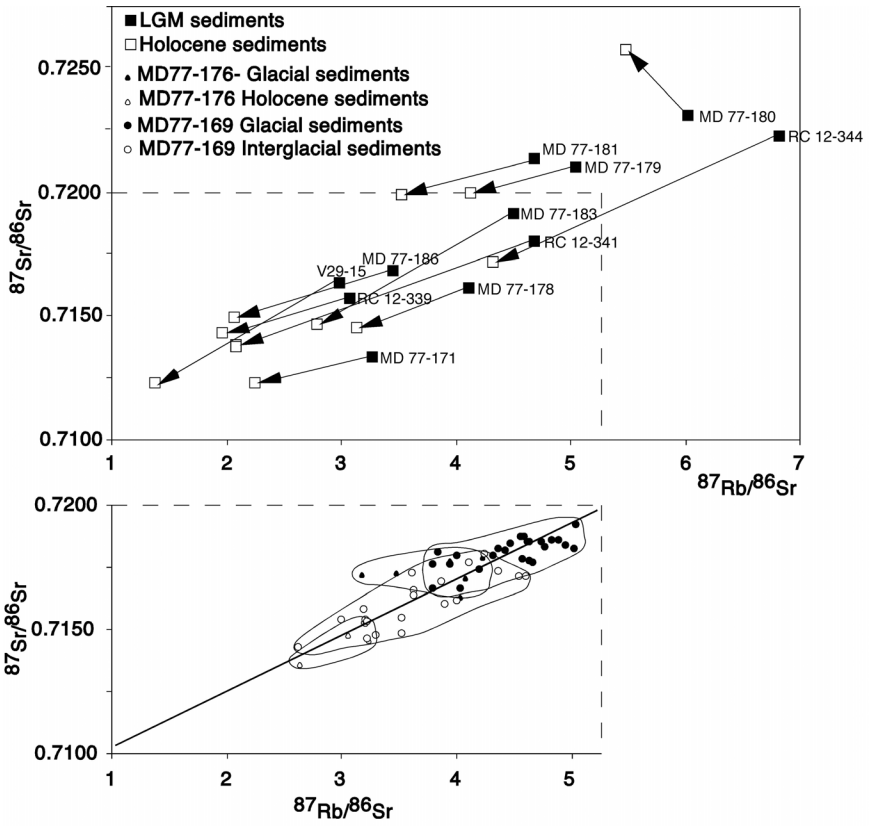

Figure 10. $^{87}Sr/^{86}Sr$ versus $^{87}Rb/^{86}Sr$ diagram indicating the isotopic distribution of both interglacial and glacial samples from cores MD77-169 and MD77-176. A compilation of previously published data for the Bay of Bengal and Andaman Sea sediments is also presented for comparison [*Colin et al.*, 1999].

depends on the behavior of the minerals in relation to the hydrolysis occurring during chemical weathering [*Clauer*, 1979]. The discussion is complicated by the fact that radiogenic $^{87}Sr^{2+}$ ions created from $^{87}Rb^{+}$ are located in a lattice configuration different from that of the nonradiogenic Sr ions incorporated during the primary crystallization of the mineral. As a consequence, Rb-rich minerals will have a tendency to preferentially release $^{87}Sr^{2+}$ upon weathering. This was exemplified by *Clauer* [1979] on lateritic soils developed on igneous rocks from La Réunion and Nosi Bé: clay minerals newly formed from both low-Rb minerals such as plagioclase and high-Rb mineral biotite exhibit $^{87}Sr/^{86}Sr$ values close to the initial ratios implying that the biotite has previously lost its radiogenic Sr. In addition, *Blum et al.* [1994] have shown that in Sierra Nevada stream waters the tendency to release radiogenic Sr is enhanced by physical erosion and concluded that biotite weathered six times more rapidly than plagioclase in the recently glaciated drainage. The initial stage of biotite alteration often involves the formation of biotite/vermiculite (or hydrobiotite) in less than 1 or 2 kyr [*Egli et al.*, 2001]. Such a transformation is associated with the release of radiogenic strontium from the bulk sediments and is often considered to significantly affect the $^{87}Sr/^{86}Sr$ ratios of major rivers draining continental shield areas [*Blum et al.*, 1994].

[46] We suggest that during glacial periods, the physical erosion of the highland Himalayas, Tibetan plateau and Indo-Burman Ranges is stronger and leads to the release of a higher quantity of unaltered K-rich minerals into the Bay of Bengal and the Andaman Sea. This physical erosion could be induced by glacial scour and frost action in the highland of the Irrawaddy and Ganges river basins. Unfortunately, the evolution of the mountain glacier during the last two glacial/interglacial cycles is not well documented for the Himalayas and Tibetan plateau. During sea level lowstands, rivers were constricted to the main channel in the lower reaches and allowed an efficient transportation by rivers of detrital minerals to the open ocean. This increase of the physical erosion is in agreement with the detrital fluxes measured in cores MD77-169, MD77-180, MD77-181 and MD77-183 (Figure 11). With the exception of core MD77-169, detrital fluxes are systematically higher during colder periods (Figure 11), suggesting a regional increase in detrital material input during glacial MIS 2, 4 and 6. Such variations in the detrital fluxes are not in agreement with the results of

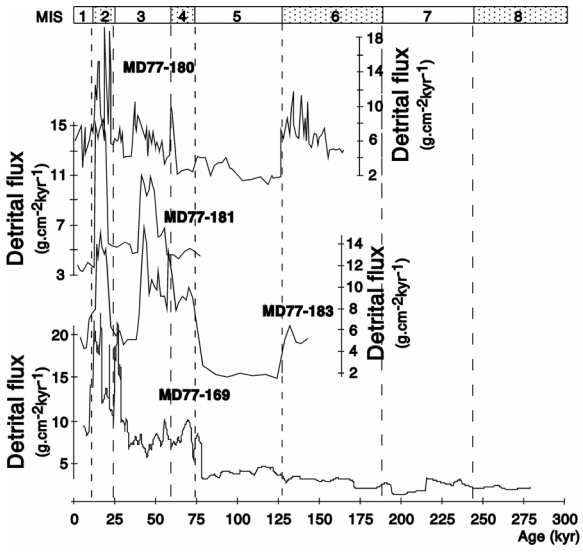

Figure 11. Variations of the detrital flux (expressed in g cm^{-2} kyr^{-1}) versus age (kyr) for cores MD77-169, MD77-180 [*Bouquillon*, 1987], MD77-181, and MD77-183 [*Fang*, 1987].

Métivier and Gaudemer [1999], which show that present-day average discharge of some largest Asian rivers has remained constant through the Quaternary (last 2 Myr). They suggest that the river network has the ability to buffer changes in hillslope erosion or sea level in order to conserve the total discharge at the outlet. At a short timescale, variations of the detrital fluxes between glacial and interglacial stages suggest a climatic control of the detrital inputs to the ocean and no major effect of buffer in floodplain.

[47] High-K minerals such as micas (radiogenic Sr composition) are very vulnerable to weathering [*Blum et al.*, 1994; *Egli et al.*, 2001], but they can be transported rapidly to the Andaman Sea and the Bay of Bengal with no strong weathering in the Irrawaddy River basin. During interglacial periods, physical erosion by mountain glacier scour is reduced and the high sea level allows the rivers to flow over a large area of the lower reaches of the Irrawaddy River basins. Detrital minerals produced by physical erosion of the highland are less efficiently transported to the ocean and experience a significant chemical weathering, which in turn induces a decrease of the $^{87}Sr/^{86}Sr$ in the detrital sediments by weathering of high-K minerals. At Milankovitch times scale, our results suggest that glacial scour and frost action in the highland of Irrawaddy River basin could have a greater impact on physical erosion than monsoon precipitations. This is not in agreement with the recent study

realized on modern Taiwan rivers showing a strong impact of the rainfall on the physical erosion [*Dadson et al.*, 2003].

[48] As climate affects the weathering of each mineral species and in particular the high-K minerals that are highly vulnerable to weathering, we suggest that glacial/interglacial changes have an important impact on the Sr isotopic compositions of the dissolved load of the river and thus can alter the net $^{87}Sr/^{86}Sr$ input into the ocean.

6. Conclusion

[49] High-resolution siliciclastic grain size, bulk and clay mineralogy combined with Sr and Nd isotopes analyses were used to establish the relationship between past changes in erosion and weathering with Indian monsoon rainfall intensity during the last 280 kyr in the eastern Tibetan Plateau and the Irrawaddy River basin.

[50] Nd isotopic investigations indicate that the Irrawaddy River has provided most of the siliciclastic materials found in the core MD77-169, which appears to be ideally suited for the study of how climate change interacts with erosion and weathering processes. Sediments from core MD77-176 result from a mixture of material deriving from the Burman Ranges and the Irrawaddy River. For both cores, $\varepsilon Nd(0)$ values do not vary significantly downcore implying no changes of the sedimentary sources through time.

[51] Variations in the kaolinite/quartz, quartz/feldspar, kaolinite/feldspar and smectite/(illite + chlorite) ratios show a strong precession periodicity suggesting that changes in Indian monsoon rainfall, rather than variations of sea level, are the main process determining mineralogical fluctuations in core MD77-169. Wet periods of summer monsoon reinforcement are characterized by an increase in these ratios. These mineralogical variations reflect an enhancement in chemical weathering of floodplain soils during wet periods of summer monsoon reinforcement.

[52] For sediments from the Andaman Sea and the eastern Bay of Bengal, glacial sediments are systematically characterized by more radiogenic $^{87}Sr/^{86}Sr$ ratios than seen in interglacial sediments. Such Sr isotopic compositions shifts are independent of the provenance of the sediments, the distance of the sediments from the supplying river mouths, and grain-size effects. The variations are interpreted as an increase of physical erosion in the highland combined with an efficient transport of detrital minerals in plain during glacial stages due to an increase in the mountain glacier extent and a sea level drop of about 120 m. Rb-rich minerals (such as biotite) vulnerable to weathering can reach the Andaman Sea and the Bay of Bengal rapidly without experiencing strong weathering. Consequently, the $^{87}Sr/^{86}Sr$ ratio alone is an ambiguous tracer of sediment provenance, because it can vary due to weathering intensity despite sediment derivation from the same source.

Acknowledgments

[53] We specially thank Peter Clift and Albert Galy for their constructive reviews, which significantly helped to improve this work. We are also grateful to Olivier Dufaure and Philippe Pradel, who helped us to process DRX. We wish to thank Giuseppe Siani for helpful discussions and comments. This manuscript is dedicated to the memory of Jacques Bertaux, who died on 26 August 2002. His contribution to the mineralogical results of this study was of primary importance.

References

Beaufort, L. (1996), Dynamics of the monsoon in the equatorial Indian Ocean over the last 260,000 years, *Quat. Int.*, *31*, 13–18.

Bender, F. (1983), *Geology of Burma*, Gebrüder Borntraeger, Berlin.

Blum, J. D., Y. Erel, and K. Brown (1994), $^{87}Sr/^{86}Sr$ ratios of Sierra Nevada stream waters: Implications for relative mineral weathering rates, *Geochim. Cosmochim. Acta*, *58*, 5019–5025.

Borg, L. E., and J. L. Banner (1996), Neodymium and strontium isotopic constraints on soil sources in Barbados, West Indies, *Geochim. Cosmochim. Acta*, *60*, 4193–4206.

Boulay, S., C. Colin, A. Trentesaux, F. Pluquet, J. Bertaux, D. Blamart, C. Buehring, and P. Wang (2003), Mineralogy and sedimentology of Pleistocene sediment in the South China Sea (ODP Site 1144), *Proc. Ocean Drill. Program Sci. Results [online]*, *184*, 1–21, (Available at http://www-odp.tamu.edu/publications/184_SR/).

Boulay, S., C. Colin, A. Trentesaux, N. Frank, and Z. Liu (2005), Sediment sources and East Asian monsoon intensity over the last 450 kyr—Mineralogical and geochemical investigations on South China Sea sediments, *Palaeogeogr. Palaeoclimatol. Palaeoecol.*, *228*, 260–277.

Bouquillon, A. (1987), Influences continentales et marines dans les sédiments Cénozoiques de l'Océan Indien Nord oriental, thesis, Univ. des Sci. et Tech. de Lille Flandres-Artois, Lille Flandres-Artois, France.

Bouquillon, A., H. Chamley, and F. Fröhlich (1989), Sédimentation argileuse au Cénozoique supérieur dans l'Océan Indien nord-oriental, *Oceanol. Acta*, *12*, 133–147.

Bouquillon, A., C. France-Lanord, A. Michard, and J. J. Tiercelin (1990), Sedimentology and isotopic chemistry of the Bengal Fan sediments: The denudation of the Himalaya, *Proc. Ocean Drill. Program Sci. Results*, *116*, 43–58.

Chamley, H. (1989), *Clay Sedimentology*, 623 pp., Springer, New York.

Chesner, C. A., W. I. Rose, A. Deino, R. Drake, and J. A. Westgate (1991), Eruptive history of Earth's largest Quaternary caldera (Toba, Indonesia) clarified, *Geology*, *19*, 200–203.

Clauer, N. (1979), Relationship between the isotopic composition of strontium in newly formed continental clay minerals and their source material, *Chem. Geol.*, *27*, 115–124.

Clemens, S. C., and W. L. Prell (1990), Late Pleistocene variability of Arabian Sea summer monsoon winds and continental aridity: Eolian records from the lithogenic component of deep-sea sediment, *Paleoceanography*, *5*(2), 109–145.

Clemens, S. C., and W. L. Prell (1991), One million year record of summer monsoon winds and continental aridity from the Owen ridge (Site 722), northwest Arabian sea, *Proc. Ocean Drill. Program Sci. Results*, *117*, 365–388.

Clemens, S. C., W. Prell, D. Murray, G. Shimmield, and G. Weedon (1991), Forcing mechanisms of the Indian Ocean monsoon, *Nature*, *353*, 720–725.

Clift, P. D., J. I. Lee, J. Blusztajn, and M. K. Clark (2002), Erosional response of South China to arc rifting and monsoonal strengthening recorded in the South China Sea, *Mar. Geol.*, *184*, 207–226.

Colin, C., C. Kissel, D. Blamart, and L. Turpin (1998), Magnetic properties of sediments in the Bay of Bengal and the Andaman Sea: Impact of rapid North Atlantic Ocean climatic events on the strength of the Indian monsoon, *Earth Planet. Sci. Lett.*, *160*, 632–635.

Colin, C., L. Turpin, J. Bertaux, A. Desprairies, and C. Kissel (1999), Erosional history of the Himalayan and Burman Ranges during the last two glacial-interglacial cycles, *Earth Planet. Sci. Lett.*, *171*, 647–660.

Dadson, S. J., et al. (2003), Links between erosion, runoff variability and seismicity in the Taiwan orogen, *Nature*, *426*, 648–651.

Dasch, E. J. (1969), Strontium isotopes in profiles, deep-sea sediments, and sedimentary rocks, *Geochim. Cosmochim. Acta*, *33*, 1521–1552.

Derry, L. A., and C. France-Lanord (1996), Neogene Himalayan weathering history and river $^{87}Sr/^{86}Sr$: Impact on the marine Sr record, *Earth Planet. Sci. Lett.*, *142*, 59–74.

Derry, L. A., and C. France-Lanord (1997), Himalayan weathering and erosion fluxes: Climate and tectonic controls, in *Tectonic Uplift and Climate Change*, edited by W. F. Ruddiman, pp. 289–312, Springer, New York.

Duplessy, J.-C. (1982), Glacial to interglacial contrasts in the northern Indian Ocean, *Nature*, *295*, 494–498.

Egli, M., A. Mirabella, and P. Fitze (2001), Clay mineral formation in soils of two different chronosequences in the Swiss Alps, *Geoderma*, *104*, 145–175.

Fagel, N., P. Debrabant, and L. André (1994), Clay supplies in the Central Indian Basin since the late Miocene: Climatic or tectonic control?, *Mar. Geol.*, *122*, 151–172.

Fang, N. (1987), Le contrôle climatique de la sédimentation Quaternaire récente dans la région moyenne du cône profond du Gange (Océan Indien), thesis, Univ. of Paris VI, Paris.

Fontugne, M., and J.-C. Duplessy (1986), Variations of the monsoon regime during the upper Quaternary: Evidence from carbon isotopic record of organic matter in north Indian Ocean sediment cores, *Palaeogeogr. Palaeoclimatol. Palaeoecol.*, *56*, 69–88.

France-Lanord, C., L. Derry, and A. Michard (1993), Evolution of the Himalaya since Miocene time: Isotopic and sedimentologic evidence from the Bengal Fan, in *Himalayan Tectonics*, edited by P. J. Treloar and M. Searle, *Geol. Soc. Spec. Publ.*, *74*, 603–621.

Galy, A., and C. France-Lanord (2001), Higher erosion rates in the Himalaya: Geochemical constraints on riverine fluxes, *Geology*, *29*, 23–26.

Gingele, F. X., P. M. Müller, and R. R. Schneider (1998), Orbital forcing of freshwater input in the Zaire Fan area—Clay mineral evidence from the last 200 kyr, *Palaeogeogr. Palaeoclimatol. Palaeoecol.*, *138*, 17–26.

Goldstein, S. J., and S. B. Jacobsen (1988), Nd and Sr isotopic systematic of river water suspended material: Implications for crustal evolution, *Earth Planet. Sci. Lett.*, *87*, 215–221.

Goldstein, S. L., R. K. O'Nions, and J. Hamilton (1984), A Sm-Nd isotopic study of atmospheric dusts and particulates from major river systems*Earth Planet. Sci. Lett.*, *70*, 221–236.

Grousset, F. E., P. E. Biscaye, A. Zindler, J. Prospero, and R. Chester (1988), Neodymium isotopes as tracers in marine sediments and aerosols: North Atlantic, *Earth Planet. Sci. Lett.*, *87*, 367–378.

Jacobsen, S. B., and G. J. Wasserburg (1980), Sm-Nd isotopic evolution of chondrites, *Earth Planet. Sci. Lett.*, *50*, 139.

Kuehl, S. A., T. M. Hariu, and W. S. Moore (1989), Shelf sedimentation off the Ganges-Brahmaputra river system: Evidence for sediment by passing to the Bengal fan, *Geology*, *17*, 1132–1135.

Liu, Z., C. Colin, A. Trentesaux, D. Blamart, F. Bassinot, G. Siani, and M.-A. Sicre (2004), Erosional history of the eastern Tibetan Plateau over the past 190 kyr: Clay mineralogical and geochemical investigations from the southwestern South China Sea, *Mar. Geol.*, *209*, 1–18.

Liu, Z., C. Colin, A. Trentesaux, G. Siani, N. Frank, D. Blamart, and S. Farid (2005), Late Quaternary climatic control on erosion and weathering in the eastern Tibetan Plateau and the Mekong Basin, *Quat. Res.*, *63*, 316–328.

Martinson, D. G., N. G. Pisias, J. D. Hays, J. Imbrie, T. C. Moore, and N. J. Shackleton (1987), Age dating and the orbital theory of the ice ages: Development of a high resolution 0 to 300,000 yr chronostratigraphy, *Quat. Res.*, *27*, 1–29.

Métivier, F., and Y. Gaudemer (1999), Stability of output fluxes of large rivers in South and East Asia during the last 2 million years: Implication on foodplain processes, *Basin Res.*, *11*, 293–303.

Nesbitt, H. W., and G. M. Young (1982), Early Proterozoic climates and plate motions inferred from major element chemistry of lutites, *Nature*, *299*, 715–717.

Oliva, P., J. Viers, and B. Dupré (2003), Chemical weathering in granitic environments, *Chem. Geol.*, *202*, 225–256.

Paillard, D., L. Labeyrie, and P. Yiou (1996), Analyseries 1.0: A Macintosh software for the analysis of geographical time-series, *Eos Trans. AGU*, *77*, 379.

Pichard, C., and F. Fröhlich (1986), Analyses IR quantitatives des sediments: Exemple du dosage du quartz et de la calcite, *Rev. Inst. Fr. Pet.*, *41*, 809–819.

Pierson-Wickmann, A.-C., L. Reisberg, C. France-Lanord, and H. R. Kudrass (2001), Os-Sr-Nd results from sediments in the Bay of Bengal: Implications for sediment transport and the marine Os record, *Paleoceanography*, *16*, 435–444.

Ségalen, P. (1995), *Les Sols Ferrallitiques et Leur Répartition Géographique*, vol. 3, ORSTOM ed., Coll. Etudes et Thèses, 201 pp., Inst. de Rech. pour le Dév., Paris.

Thiry, M. (2000), Palaeoclimatic interpretation of clay minerals in marine deposits: An outlook from the continental origin, *Earth Sci. Rev.*, *49*, 201–221.

Tütken, T., A. Eisenhauer, B. Wiegand, and B. T. Hansen (2002), Glacial-interglacial cycles in Sr and Nd isotopic

composition of Arctic marine sediments triggered by the Svalbard/barents Sea ice sheet, *Mar. Geol.*, *182*, 351–372.

Weber, M. E., M. Wiedicke-Hombach, H. R. Kudrass, and H. Erlenkeuser (2002), Bengal Fan sediment transport activity and response to climate forcing inferred from sediment physical properties, *Sediment. Geol.*, *30*, 69.

Webster, P. J. (1987), *The Elementary Monsoon*, pp. 3–32, John Wiley, Hoboken, N. J.

Wehausen, R., and H.-J. Brumsack (2002), Astronomical forcing of the East Asian monsoon mirrored by the composition of Pliocene South China Sea sediments, *Earth Planet. Sci. Lett.*, *201*, 621–636.